ACS APPLIED MATERIALS & INTERFACES

Research Article

www.acsami.org

Facile Preparation of Well-Dispersed CeO_2–ZnO Composite Hollow Microspheres with Enhanced Catalytic Activity for CO Oxidation

Qingshui Xie,[†] Yue Zhao,[‡] Huizhang Guo,[†] Aolin Lu,[†] Xiangxin Zhang,[†] Laisen Wang,[†] Ming-Shu Chen,[‡] and Dong-Liang Peng*,[†]

[†]Department of Materials Science and Engineering, College of Materials, Fujian Key Laboratory of Advanced Materials, Xiamen University, Xiamen 361005, China

[‡]State Key Laboratory of Physical Chemistry of Solid Surfaces, National Engineering Laboratory for Green Chemical Productions of Alcohols-Ethers-Esters, Department of Chemistry, College of Chemistry and Chemical Engineering, Xiamen University, Xiamen 361005, China

Supporting Information

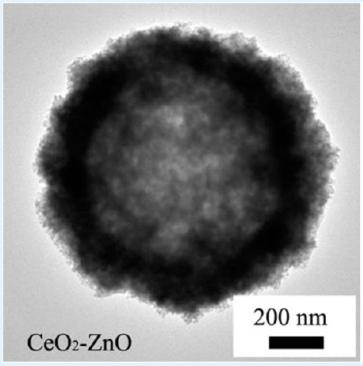

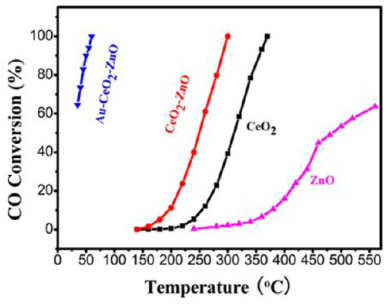

ABSTRACT: In this article, well-dispersed CeO_2–ZnO composite hollow microspheres have been fabricated through a simple chemical reaction followed by annealing treatment. Amorphous zinc–cerium citrate hollow microspheres were first synthesized by dispersing zinc citrate hollow microspheres into cerium nitrate solution and then aging at room temperature for 1 h. By calcining the as-produced zinc–cerium citrate hollow microspheres at 500 °C for 2 h, CeO_2–ZnO composite hollow microspheres with homogeneous composition distribution could be harvested for the first time. The resulting CeO_2–ZnO composite hollow microspheres exhibit enhanced activity for CO oxidation compared with CeO_2 and ZnO, which is due to well-dispersed small CeO_2 particles on the surface of ZnO hollow microspheres and strong interaction between CeO_2 and ZnO. Moreover, when Au nanoparticles are deposited on the surface of the CeO_2–ZnO composite hollow microspheres, the full CO conversion temperature of the as-produced 1.0 wt % Au–CeO_2–ZnO composites reduces from 300 to 60 °C in comparison with CeO_2–ZnO composites. The significantly improved catalytic activity may be ascribed to the strong synergistic interplay between Au nanoparticles and CeO_2–ZnO composites.

KEYWORDS: *zinc–cerium citrate, CeO_2, ZnO, composite hollow microspheres, catalytic oxidation*

INTRODUCTION

Hollow structures have been widely investigated in recent years due to their low density and high specific surface area, which may find applications in catalysis, lithium ion batteries, drug delivery, and so on.[1−9] For example, Lou's group reported the successful synthesis of V_2O_5 hollow microspheres which revealed excellent electrochemical properties in lithium ion batteries.[7] Yolk-shell TiO_2 hollow microspheres fabricated by Li et al. demonstrated superior photocatalytic activity for phenol degradation.[8] To date, the majority of research has focused on the control of the shape and interior cavity of single oxide hollow structures. Very recently, some studies have found that the mixed metal oxides possess enhanced or novel physical and/or chemical properties through the synergistic effect.[10−16] In other words, the properties of the mixed metal oxides cannot be regarded as a simple superposition of the single oxides. For example, ZnO nanorod–SnO_2 nanoparticle heterostructures revealed significantly enhanced catalytic activity than pure ZnO nanorods.[15] He's group synthesized NiO–ZnO hybrid nanofibers which showed better electrochemical performances than pure NiO and ZnO nanofibers.[16] However, up to now, the mixed metal oxides with well-defined hollow structures have rarely been reported due to the complicated procedures and severe reaction conditions.

The catalytic oxidation of CO to CO_2 has received intense attention over the last three decades owing to its potential

Received: October 12, 2013
Accepted: December 4, 2013
Published: December 4, 2013

applications such as automotive exhausts, gas sensors, CO_2 lasers, and fuel cells, as well as for an ideal model reaction for surface science investigations.[17−19] For example, in the proton exchange membrane fuel cells (PEMFCs), the trace amount of CO would lead to poisoning of Pt-based electrodes. Thus, CO preferential oxidation in a hydrogen-rich gas has been regarded as one of the most promising solutions for complete CO removal. Among various inorganic oxide catalysts, CeO_2 has attracted extensive interest due to its high thermal stability, oxygen storage capacities, and easy conversion between Ce(III) and Ce(IV) oxidation states.[20−23] Various morphologies of CeO_2 micro/nanostructures, such as nanotubes, nanoparticles, nanocubes, and hollow spheres, have been successfully synthesized and used for CO catalytic oxidation.[24−28] On the other hand, ZnO is an attractive semiconductor, which has attracted extensive research interest for its potential applications.[29] Compared to other oxides, although ZnO has been less investigated for the CO catalytic oxidation, increasing attention toward ZnO employed as a support can be found in the latest years.[30−32] Recently, research has demonstrated that $Ce_{1-x}Zn_xO_{2-\theta}$ solid solution nanodisks show higher catalytic activity for CO oxidation than pure CeO_2.[33] Therefore, it is desirable to develop CeO_2−ZnO composite hollow microspheres that can be used as catalysts or catalyst supports to completely oxidize CO at lower temperature.

Herein, we report the successful fabrication of crystalline CeO_2−ZnO composite hollow microspheres via annealing of amorphous zinc−cerium citrate hollow microspheres synthesized through a simple chemical reaction. The effect of the annealing temperature on the morphology and structure of the as-acquired composites was investigated. The obtained well-dispersed CeO_2−ZnO composite hollow microspheres exhibit excellent catalytic activity for CO oxidation. In order to further improve the CO catalytic activity, Au−CeO_2−ZnO composite hollow microspheres were prepared through the deposition of Au nanoparticles on the surface of CeO_2−ZnO composite hollow microspheres.

EXPERIMENTAL SECTION

Synthesis. Amorphous zinc citrate hollow microspheres were first produced through a simple approach, as shown in our earlier literature.[34] In a typical synthesis process, a mixed aqueous solution (50 mL) composed of 0.149 g of $Zn(NO_3)_2{\cdot}6H_2O$, 0.035 g of $(CH_2)_6N_4$, and 0.04 g of $K_3C_6H_5O_7{\cdot}H_2O$ was kept in a water bath at 90 °C for 20 min, followed by aging at room temperature for 12 h. After that, white zinc citrate hollow microspheres can be harvested by centrifugation and rinsed with deionized water and ethanol three times. Subsequently, 30 mL of cerium nitrate suspension contained 0.06 g of the as-obtained zinc citrate hollow microspheres was sonicated for 10 min and then aged at room temperature for 1 h. The gray zinc−cerium citrate precursor was centrifuged, washed with deionized water three times, and then dried at 80 °C for 10 h. Finally, the well-dispersed CeO_2−ZnO composite hollow microspheres were gained by calcination of zinc−cerium citrate precursor at 500 °C for 2 h in air.

Au nanoparticles were deposited on the surface of CeO_2−ZnO composite hollow microspheres by the deposition−precipitation method. First, CeO_2−ZnO composite hollow microspheres (0.2 g) were dispersed in 5 mL of deionized water under ultrasonic conditions to form a uniform suspension. Then, 5 mL of $HAuCl_4$ solution was added into the above suspension drop by drop under vigorous stirring. Afterward, the pH value of the mixed solution was adjusted to 10 using 0.2 M NaOH solution. Then, the resulting suspension was aged at room temperature for 12 h under magnetic stirring. Finally, Au−CeO_2−ZnO composites were acquired by centrifugation and rinsed with hot deionized water several times until no Cl^- ions are detectable using $AgNO_3$ solution and then dried at 100 °C for 12 h.

Characterization. The crystal phases of the as-obtained products were measured on a PANalytical X' pert PRO X-ray diffractometer using Cu Kα radiation (40 kV, 60 mA). A LEO-1530 field-emission scanning electron microscope and JEM-2100 transmission electron microscope operated at 200 kV were employed to characterize the detailed morphology and microstructures of the samples. The thermogravimetric (TG) investigation was performed on a Du Pont Instrument 1090B thermal analyzer. A Nicolet Nexus-670 FT-IR spectrometer was applied to gain the Fourier-transform infrared (FTIR) spectra of zinc−cerium citrate hollow microspheres. X-ray photoelectron spectra (XPS) were acquired from a Qtac-100 LEISS-XPS Instrument. A TriStar 3020 system was employed to characterize the Brunauer−Emmett−Teller (BET) surface area of the samples. A Cary 500 UV−vis−NIR spectrophotometer was used to measure the UV−vis diffuse reflectance (DR) spectra of the samples. The Au content of Au−CeO_2−ZnO composites was determined by an inductively coupled plasma mass spectrometer (ICP-MS-4500).

Catalytic Measurements. The CO catalytic oxidation was carried out in a fixed-bed flow reactor with an inside diameter of 6 mm at atmospheric pressure. 100 mg of the as-produced samples was added into the reactor. A gas mixture composed of $CO/O_2/H_2/He$ (0.5:0.5:50:49) with a total flow rate of 50 mL/min flowed through the reactor. The catalytic temperature was controlled by an electrical furnace with a heating rate of 2 °C/min. At each temperature interval (20 °C), the catalytic reaction was conducted for 5 min to reach the reaction equilibrium. Then, the composition of the effluent gas was measured on a gas chromatograph equipped with a flame ionization detector. The CO conversion ratio was determined on the basis of the CO consumption and CO_2 formation.

RESULTS AND DISCUSSION

The SEM and TEM images of the zinc−cerium citrate precursor are demonstrated in Figure 1. From a panoramic SEM micrograph, as shown in Figure 1a, it can be observed that the precursor is made up of dispersed microspheres with an average diameter on the order of 1.35 μm. A cracked sphere

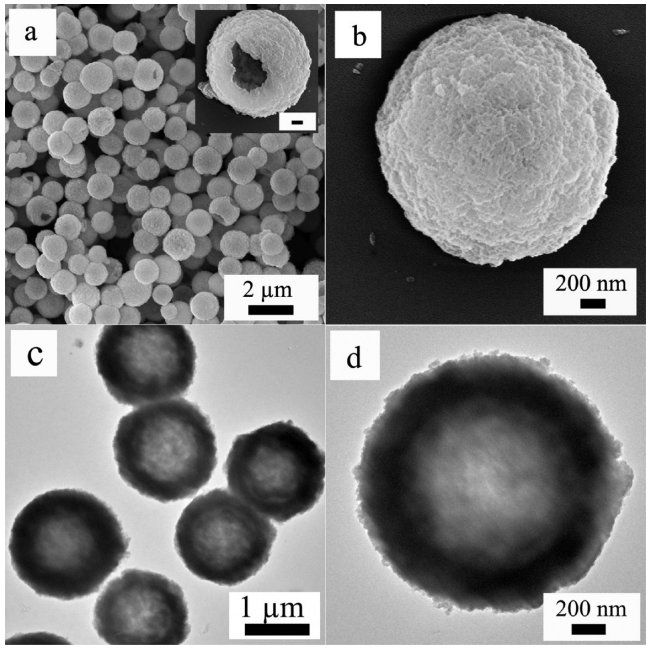

Figure 1. The panoramic (a) and magnified (b) SEM images for zinc−cerium citrate hollow microspheres. The inset manifests a cracked microsphere, and the scale bar is 100 nm. The low (c) and high (d) magnified TEM images for zinc−cerium citrate hollow microspheres.

dx.doi.org/10.1021/am404487b | ACS Appl. Mater. Interfaces 2014, 6, 421−428

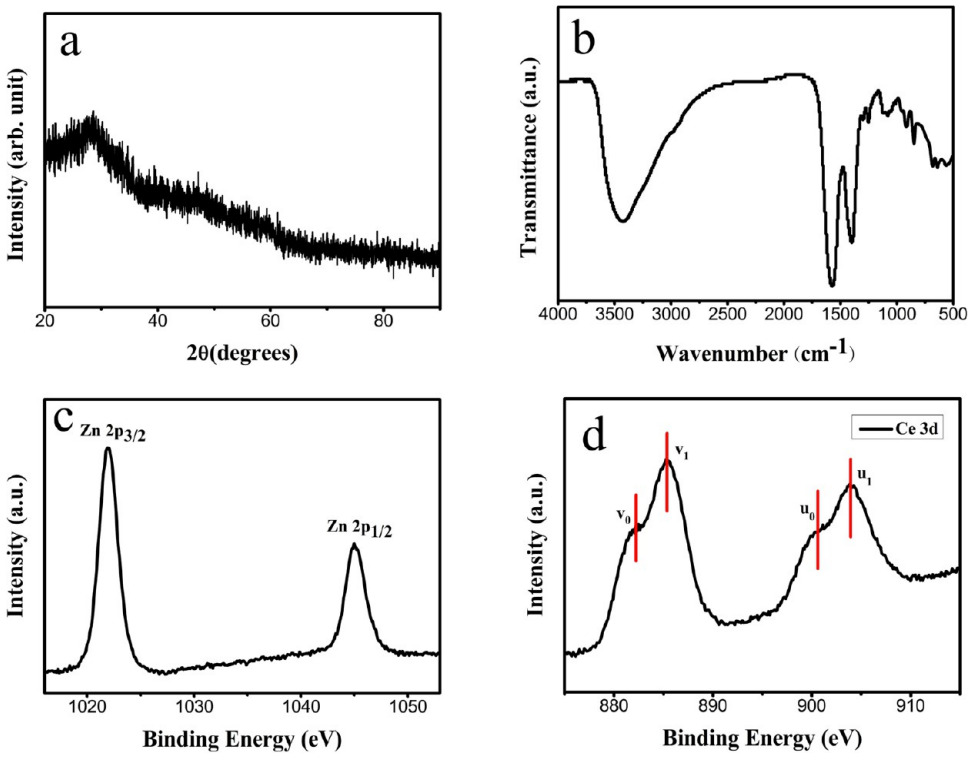

Figure 2. XRD pattern (a), FT-IR spectrum (b), and Zn 2p (c) and Ce 3d (d) high-resolution XPS spectra for the as-produced zinc−cerium citrate.

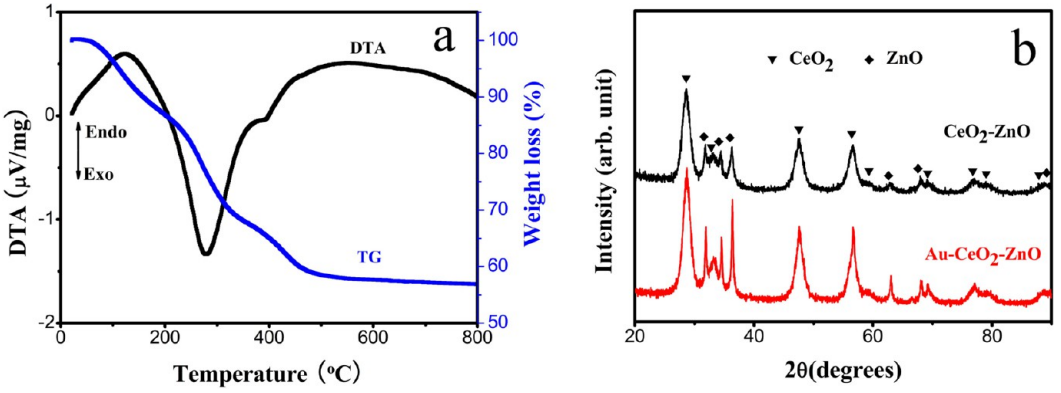

Figure 3. (a) TG and DTA curves for zinc−cerium citrate. (b) The XRD patterns of CeO_2−ZnO and Au−CeO_2−ZnO composite hollow microspheres.

(the inset in Figure 1a) shows the interior cavity of the microsphere. The magnified SEM image manifests the relative coarse and loose surface of the microsphere (Figure 1b). The Ce/Zn ratio of the precursor is determined to be about 1 (EDS, Figure S1, Supporting Information). The hollow structure of the precursor is also evidenced from the TEM images, as displayed in Figure 1c and d. The hollow microspheres have a shell thickness of about 300 nm. From the powder XRD pattern (Figure 2a), it can be found that the as-obtained zinc−cerium citrate composite hollow microspheres are amorphous. The FT-IR spectrum (Figure 2b) of zinc−cerium citrate hollow microspheres reveals two mighty and aculeated absorption peaks located at 1573 and 1398 cm^{-1}, originating from the stretching vibrations of carboxylate groups for the coordinated citrates.[35−37] The large peak centered at 3436 cm^{-1} is due to the vibrations of −OH groups. The full XPS spectrum of zinc−cerium citrate hollow microspheres (Figure S2, Supporting Information) suggests that the precursor contains four elements including Zn, Ce, O, and C. The high-resolution Zn 2p spectrum (Figure 2c) demonstrates two peaks centered at 1021.6 and 1045.2 eV, which can be assigned to Zn $2p_{3/2}$ and Zn $2p_{1/2}$ of Zn(II), respectively. The high-resolution Ce 3d spectrum is displayed in Figure 2d. The Ce 3d electron core level can be divided into two peaks: $3d_{5/2}$ and $3d_{3/2}$, marking as "u" and "v" peaks, respectively. From the Ce 3d spectrum of the precursor, only v_0, v_1, u_0, and u_1 peaks stemming from Ce(III) can be observed, which verifies the Ce(III) oxidation state of the precursor.[38] The O 1s peak (Figure S3, Supporting Information) located at 530.6 eV arises from the lattice oxygen, while the peak centered at 531.5 eV is ascribed to the surface hydroxyl groups.[13] On the basis of the above results and analysis, it is reasonable to affirm that the as-obtained precursor is zinc−cerium(III) citrate.

Zinc−cerium citrate composites were further investigated by TG/DTA analysis (Figure 3a). The first weight loss at a temperature below 200 °C results from the removal of

dx.doi.org/10.1021/am404487b | ACS Appl. Mater. Interfaces 2014, 6, 421−428

adsorbed water. The subsequent weight loss of 19.2% between 210 and 360 °C arises from the conversion of zinc citrate to ZnO, corresponding to a strong exothermic peak near 276 °C in the DTA curve. About 9.4% of weight loss can be clearly discerned in the range 360−500 °C in the TG curve, attributing to the decomposition of cerium(III) citrate to CeO_2. No more weight loss takes place with further increase of the temperature, suggesting the complete transformation of zinc−cerium citrate hollow microspheres into CeO_2−ZnO composite hollow microspheres. Shown in Figure 3b is the XRD pattern of the product after calcination of zinc−cerium citrate at 500 °C for 2 h. All the diffraction peaks can be indexed to hexagonal ZnO (JCPDS card no. 36-1451) and cubic CeO_2 (JCPDS-34-0394). No additional impurity peaks can be seen, implying the high purity of the product. The broadening of the diffraction peaks is attributed to the small ZnO and CeO_2 crystal particles. The average grain sizes of CeO_2 and ZnO powders are approximately 9.6 and 16.2 nm determined by the Scherrer equation, respectively.

The SEM and TEM investigations (Figure 4) manifest that CeO_2−ZnO composites calcined at 500 °C are composed of dispersed hollow microspheres with an average diameter of about 1.0 μm. A cracked sphere is depicted in the inset of Figure 4a. The interior void space can be clearly observed. Each CeO_2−ZnO microsphere is made up of numerous particles with particle sizes ranging from 8 to 20 nm (Figure 4b). Particle size values observed from the SEM macrograph are consistent with the XRD results. Furthermore, the outstanding interfacial contact can be envisaged due to the tight connection between CeO_2 and ZnO nanoparticles (Figure 4b). The hollow structure of CeO_2−ZnO composites with an average shell thickness of 210 nm is visible from the TEM characterization shown in Figure 4c and d. The corresponding SAED pattern (Figure 4e) suggests the simultaneous presence of CeO_2 and ZnO. The content of cerium in the CeO_2−ZnO composites after calcination remains almost unchanged in comparison with zinc−cerium citrate (Figure S4, Supporting Information). The high-angle annular dark-field (HAADF) scanning TEM (STEM) image (Figure 4f) further verifies the hollow structure of the product. The elemental mappings of Ce, Zn, and O obtained from the square region in Figure 4f are manifested in Figure 4g, h, and i, respectively. Notably, CeO_2 and ZnO are homogeneously distributed in the CeO_2−ZnO composites. The HAADF-STEM cross-sectional compositional line profiles (Figure S5, Supporting Information) of a CeO_2−ZnO composite hollow microsphere reveal stronger Zn and Ce signals at the edge of the microsphere than the center, which also clearly demonstrate the hollow structure of the obtained CeO_2−ZnO composites.

The effect of calcination temperature on the morphology and structures of CeO_2−ZnO composites was investigated. The XRD measurement (Figure S6, Supporting Information) suggests that both of the obtained products by calcination of zinc−cerium citrate precursor at 650 and 800 °C are CeO_2−ZnO composites, which indicates that the increase of annealing temperature would not change the crystal phases of the products. The significantly strengthened diffraction peaks imply the better crystallinity of the composites calcined at higher temperature. The average grain sizes of CeO_2 and ZnO acquired at 650 and 800 °C are approximately 12.4/16.9 and 25.1/19.9 nm based on the Scherrer equation, respectively. The SEM and TEM characterizations were also conducted, and the results are displayed in Figure 5. The hollow structures of the

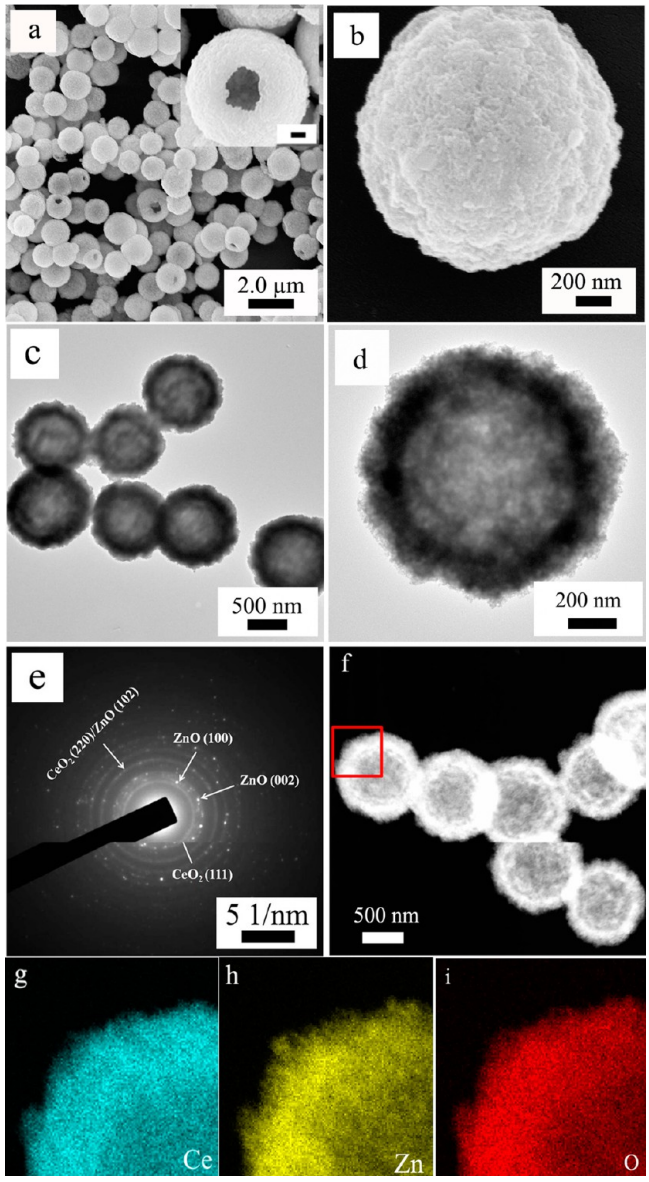

Figure 4. The panoramic (a) and magnified (b) SEM micrographs of CeO_2−ZnO composites obtained by calcination of zinc−cerium citrate hollow microspheres at 500 °C. The inset reveals a cracked sphere, and the scale bar is 100 nm. The low (c) and high (d) magnified TEM images of CeO_2−ZnO composites. (e) The corresponding SAED pattern of CeO_2−ZnO composite hollow microspheres. (f) HAADF image of CeO_2−ZnO composite hollow microspheres. Elemental mappings of Ce (g), Zn (h), and O (i) obtained from the square region in part f.

obtained composites calcined at 650 and 800 °C remain unchanged. However, some particle aggregates indicated by black arrows in Figure 5a and c form with increasing annealing temperature from 500 to 650 and 800 °C. Moreover, the particle sizes observed from the magnified SEM images (Figure 5b and d) are also significantly increased, which is in agreement with the above XRD results. Consequently, it is reasonable to pronounce that the annealing temperature plays an important role in the morphology of the obtained composites. The well-dispersed CeO_2−ZnO composite hollow microspheres without the formation of individual aggregates can be synthesized by calcination of zinc−cerium citrate hollow microspheres at 500 °C.

dx.doi.org/10.1021/am404487b | ACS Appl. Mater. Interfaces 2014, 6, 421−428

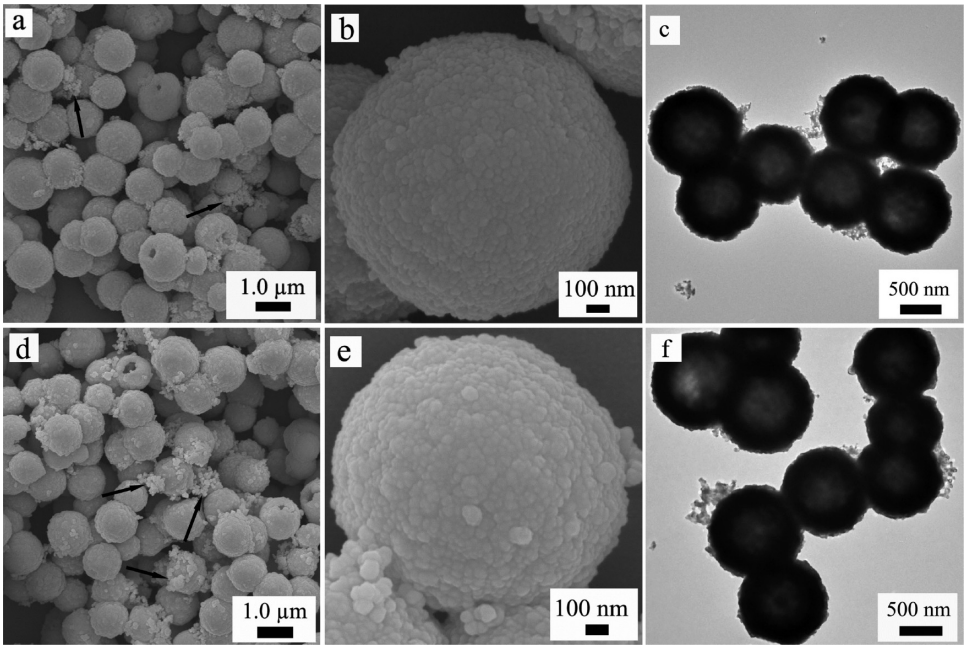

Figure 5. The SEM and TEM images of CeO_2–ZnO composites synthesized by calcination of zinc–cerium citrate hollow microspheres at 650 °C (a–c) and 800 °C (d–f).

CO catalytic oxidation was carried out to evaluate the catalytic performance of the obtained products. For comparison, ZnO hollow microspheres prepared by calcining the original zinc citrate hollow microspheres at 500 °C for 2 h and commercial CeO_2 particles are also characterized for the CO catalytic oxidation. The results for the above samples are plotted in Figure 6. The gradual increase of conversion ratio

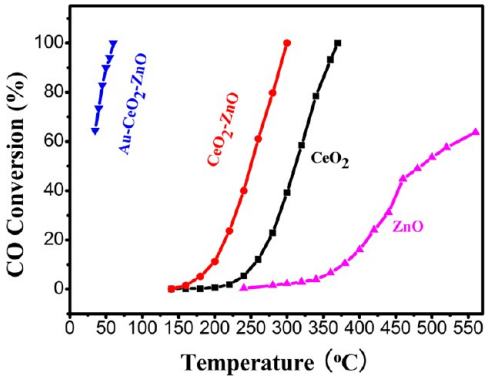

Figure 6. The CO conversion percentage for CeO_2–ZnO composite hollow microspheres calcined at 500 °C, 1 wt % Au–CeO_2–ZnO composite hollow microspheres, ZnO hollow microspheres, and commercial CeO_2 powders.

with increasing reaction temperature indicates more and more CO is oxidized. The complete CO oxidation can be acquired at 300 °C for the CeO_2–ZnO composite hollow microspheres calcined at 500 °C, which is 70 °C lower than that of the commercial CeO_2 powders. ZnO hollow microspheres possess the lowest catalytic efficiency, which shows only 50% CO conversion as the temperature reaches as high as 500 °C. Furthermore, the catalytic properties of CeO_2–ZnO, CeO_2, and ZnO powders are normalized by the Brunauer–Emmett–Teller (BET) surface area. N_2 adsorption–desorption isotherms of CeO_2–ZnO, CeO_2, and ZnO powders are displayed in Figure S7 (Supporting Information), which suggest specific surface areas of 40.9, 77.8, and 16.4 $m^2\ g^{-1}$, respectively. The specific rates of the CO oxidation for CeO_2–ZnO, CeO_2, and ZnO powders at 300 °C are about 150.4, 31.2, and 8.1 μmol $(m^2)^{-1}\ h^{-1}$, respectively. CeO_2–ZnO composite hollow microspheres possess the fastest CO oxidation rate as compared with ZnO hollow microspheres and CeO_2 powders. In addition, a straightforward comparison of CO catalytic activity for various CeO_2 hollow structures is summarized and listed in Table 1. For example, Yang's group reported the

Table 1. A Rough Comparison of CO Catalytic Activity for Various CeO_2 Hollow Structures

morphology	total CO conversion temperature	ref
hollow nanospheres	320 °C	39
nanotubes arrays	500 °C	24
hollow nanospheres	400 °C	40
hollow nanocrystals	>300 °C	26
hollow spheres	490 °C	28
our work	300 °C	

successful preparation of CeO_2 hollow nanospheres by the hydrothermal route, which revealed the full CO conversion at 320 °C.[39] CeO_2 nanotube arrays fabricated by Feng showed the complete oxidation of CO at 500 °C.[24] Shen et al. synthesized CeO_2 hollow spheres by the self-template hydrothermal method, which fully oxidized CO at 490 °C.[28] Compared with other CeO_2 hollow structures, the well-dispersed CeO_2–ZnO composite hollow microspheres prepared in our work exhibit enhanced CO catalytic activity, which is due to the synergistic effect between CeO_2 and ZnO. A schematic formation process of the well-dispersed CeO_2–ZnO composite hollow microspheres is illustrated in Figure 7. The IR result (Figure 2b) has validated the presence of –OH and $-COO^-$ functional groups in the initial zinc citrate hollow microspheres. The adsorption of metal ions on the surfaces of zinc citrate

dx.doi.org/10.1021/am404487b | ACS Appl. Mater. Interfaces 2014, 6, 421–428

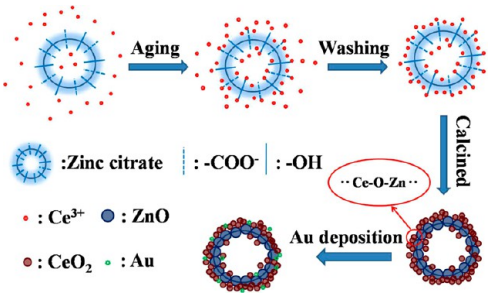

Figure 7. Schematic formation process of well-dispersed CeO_2−ZnO composite hollow microspheres.

hollow microspheres is anticipated through the electrostatic interactions between metal ions and surface functional groups. Therefore, when cerium nitrate suspension containing zinc citrate hollow microspheres was aged at room temperature, the adsorption of Ce^{3+} ions on the coarse surfaces of zinc citrate hollow microspheres takes place. The superfluous unadsorbed Ce^{3+} ions would be removed during the subsequent washing process. Due to the anchor effect of surface hydrophilic groups, the adsorbed Ce^{3+} ions would function as the in situ cerium source to synthesize CeO_2 nanoparticles which well disperse on the surfaces of the resulting ZnO hollow microspheres without the formation of individual aggregates under heat treatment at 500 °C for 2 h.[41] Simultaneously, a good interfacial contact between CeO_2 and ZnO nanoparticles would form legitimately. Then, more Ce−O−Zn linkages may be formed at the interface between CeO_2 and ZnO nanoparticles, leading to strengthening interfacial interactions and more easily adsorbing CO.[42] Consequently, the CO catalytic activity of CeO_2−ZnO composite hollow microspheres is greatly improved through the synergistic effect between CeO_2 and ZnO. Additionally, CeO_2−ZnO composite catalyst after the catalytic reaction at 300 °C was recovered to further characterize its stability. The XRD pattern and TEM image (Figure S8, Supporting Information) demonstrate that the crystal phase and the hollow structure of CeO_2−ZnO composite catalyst are well preserved after the catalytic reaction, implying the good stability of the as-produced composite catalysts.

In order to further improve CO catalytic activity, Au nanoparticles were deposited on the surfaces of CeO_2−ZnO composite hollow microspheres by the deposition−precipitation method. As shown in Figure 3b, it is visible that the crystal phases of CeO_2−ZnO composites after loading of Au nanoparticles keep almost unchanged in comparison with initial CeO_2−ZnO composites. Furthermore, no characteristic peaks arising from metallic gold or gold oxide species can be observed, indicating the low content and highly dispersed Au nanoparticles on the surfaces of CeO_2−ZnO composite hollow microspheres.[43] The Au, CeO_2, and ZnO content in the Au−CeO_2−ZnO composites was about 1.0, 48.9, and 50.1 wt %, respectively, as determined by inductively coupled plasma mass spectrometry. Figure 8a reveals the TEM image of the as-obtained Au−CeO_2−ZnO composites, which remain as hollow structures after the deposition of Au nanoparticles. However, Au nanoparticles could not be clearly discerned due to small

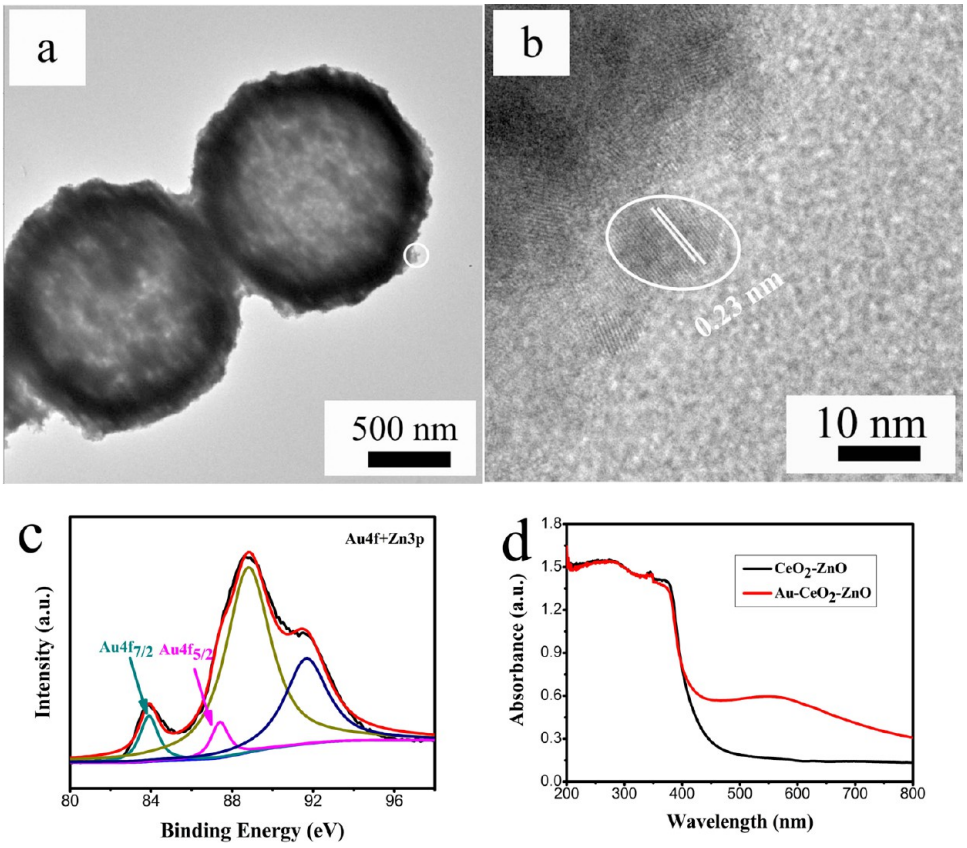

Figure 8. (a) The TEM image of 1 wt % Au−CeO_2−ZnO composite hollow microspheres. (b) The HRTEM micrograph of the shell area indicated by a circle in part a. (c) Au 4f high-resolution XPS spectrum for 1 wt % Au−CeO_2−ZnO composite hollow microspheres. (d) UV−visible absorption spectra of 1 wt % Au−CeO_2−ZnO and CeO_2−ZnO composite hollow microspheres.

dx.doi.org/10.1021/am404487b | ACS Appl. Mater. Interfaces 2014, 6, 421−428

particle sizes and the relatively thick shells of CeO_2−ZnO composite hollow microspheres. From the HRTEM image (Figure 8b), the measured interplanar distances of 0.23 nm achieved from the circled region in Figure 8a are ascribed to the lattice spacing of the (111) plane of Au. Shown in Figure 8c is the XPS spectrum of the Au 4f region for Au−CeO_2−ZnO composites, which reveals the partial superposition between Au4f and Zn3p peaks. The XPS spectrum can be divided into four peaks. The peaks located at 83.7 and 87.4 eV can be assigned to the $Au4f_{7/2}$ and $Au4f_{5/2}$, respectively, implying the metallic Au^0 state. Moreover, a 0.3 eV negative shift of Au^04f (from 84.0 to 83.7 eV) can be observed, which is due to the strong interactions between Au nanoparticles and CeO_2−ZnO supports.[44] UV−vis absorption spectra of Au−CeO_2−ZnO and CeO_2−ZnO composites are shown in Figure 8d. Compared to CeO_2−ZnO supports, an additional absorption peak round 560 nm for Au−CeO_2−ZnO composites is visible, creating by the absorption of Au nanoparticles.[45] It is well accepted that Au nanoparticles reveal surface plasmon resonance absorption near 520 nm.[38,46,47] The observed red shift may be due to the strong interplay between Au nanoparticles and CeO_2−ZnO supports, which is consistent with the XPS result (Figure 8c).[44] The BET surface area of Au−CeO_2−ZnO composite hollow microspheres is about 32.4 $m^2\ g^{-1}$, which decreases slightly compared with CeO_2−ZnO composite hollow microspheres (Figure S7, Supporting Information). The obtained Au−CeO_2−ZnO composite hollow microspheres show good catalytic activity at room temperature with a CO conversion ratio of about 60% (Figure 6). In comparison with CeO_2−ZnO composite hollow microspheres, the temperature of CO complete oxidation for Au−CeO_2−ZnO composite hollow microspheres significantly decreases from 300 to 60 °C. Also, the effect of Au content in Au−CeO_2−ZnO composites on the CO catalytic activity was carried out. Two Au−CeO_2−ZnO composites with Au contents of about 0.48 and 1.91 wt % were fabricated by simply adjusting the dosage of $HAuCl_4$ under the same deposition−precipitation method. As depicted in Figure S9 (Supporting Information), the CO catalytic activity order is suggested as follows: 1.0 wt % Au−CeO_2−ZnO > 1.91 wt % Au−CeO_2−ZnO > 0.48 wt % Au−CeO_2−ZnO. It can be obviously found that the amount of Au in Au−CeO_2−ZnO composites plays an important role in the CO catalytic oxidation. First, the increase of the Au contents can effectively increase the active sites for CO catalytic oxidation, giving rise to the improvement of catalytic activity. However, with further increase in the amount of Au, Au particles may significantly grow up, which is bad for the CO catalytic oxidation.[23,48,49] Therefore, 1.0 wt % Au−CeO_2−ZnO composites possess the highest CO catalytic activity compared with other counterparts. Impressively, the obtained 1.0 wt % Au−CeO_2−ZnO composite hollow microspheres reveal one of the best CO catalytic properties among the Au−$Ce_{1-x}Zn_xO_{2-\theta}$, Au−CeO_2, and Au−ZnO catalysts reported recently.[23,32,33,38−40] For example, Zhong et al. prepared the Au−$CeZnO_3$ nanocomposites with a total CO conversion at 85 °C.[33] Tang's group reported the successful fabrication of core−shell Au@CeO_2 nanocomposites with a similar content of Au, which revealed the full CO conversion at 155 °C.[23] Au−ZnO nanocatalysts synthesized by Carabineiro demonstrated the complete CO oxidation at 200 °C.[32] The greatly enhanced catalytic activity is attributed to the strong interfacial interactions between Au nanoparticles and CeO_2−ZnO supports. As discussed above, small CeO_2 nanoparticles are well dispersed on the surfaces of ZnO hollow microspheres in the CeO_2−ZnO composites and numerous Ce−O−Zn linkages may be formed at the interface between CeO_2 and ZnO nanoparticles (Figure 7). It is well accepted that CeO_2 is rich in oxygen vacancy defects and has a large oxygen storage capacity, which is beneficial for the CO catalytic oxidation.[38] Accordingly, acid (Zn^{2+}) and basic (O^{2-}) surface sites make ZnO a good support for Au deposition.[30] As a result, the synergistic effect between CeO_2 and ZnO nanoparticles facilitates the adsorption of CO and the deposition of Au nanoparticles. Furthermore, the hollow structures are favorable for the dispersion of Au nanoparticles on the surfaces of CeO_2−ZnO composite hollow microspheres.[38] Thus, the interaction between Au nanoparticles and CeO_2−ZnO supports is greatly strengthened, which is consistent with the XPS and UV−vis absorption results (Figure 8c and d). Consequently, Au−CeO_2−ZnO composite hollow microspheres reveal significantly enhanced CO catalytic activity.

CONCLUSIONS

A simple strategy was employed to synthesize well-dispersed CeO_2−ZnO composite hollow microspheres via calcining an amorphous zinc−cerium citrate hollow precursor. The annealing temperature plays an important role in the morphology of the obtained composites. The CO catalytic activity of the obtained CeO_2−ZnO composite hollow microspheres calcined at 500 °C is significantly enhanced through the synergistic effect in comparison with ZnO hollow microspheres and commercial CeO_2 powders. Furthermore, the as-produced 1.0 wt % Au−CeO_2−ZnO composite hollow microspheres reveal superior catalytic activity with full CO conversion at 60 °C, which may be ascribed to the high dispersion of Au nanoparticles and strong interfacial interaction between Au nanoparticles and CeO_2−ZnO supports. The facile synthetic strategy should also be employed to prepare other mixed metal oxides with well-defined hollow structure which may find potential applications in the catalysis and energy area.

ASSOCIATED CONTENT

Supporting Information

Additional EDS and XPS spectra of zinc−cerium citrate hollow microspheres, EDS spectrum, and the HAADF-STEM cross-sectional compositional line profiles of CeO_2−ZnO composites. The XRD patterns of CeO_2−ZnO composites calcined at 650 and 800 °C. N_2 adsorption−desorption isotherms of the obtained samples. The XRD pattern and TEM image of CeO_2−ZnO composites after catalytic reaction. CO catalytic activity of Au−CeO_2−ZnO composites with different amounts of Au. This material is available free of charge via the Internet at http://pubs.acs.org.

AUTHOR INFORMATION

Corresponding Author

*E-mail: dlpeng@xmu.edu.cn.

Notes

The authors declare no competing financial interest.

ACKNOWLEDGMENTS

The authors gratefully acknowledge financial support from the National Basic Research Program of China (Grant No. 2012CB933103), National Outstanding Youth Science Foundation of China (Grant No. 50825101), the National Natural

Science Foundation of China (Grant Nos. 51171158, 51371154, and 51301145), and the Fundamental Research Funds for the Central Universities of China (Grant No. 201212G001).

REFERENCES

(1) Liu, Y.; Yu, L.; Hu, Y.; Guo, C. F.; Zhang, F. M.; Lou, X. W. *Nanoscale* **2012**, *4*, 183−187.
(2) Kim, J.; Piao, Y.; Hyeon, T. *Chem. Soc. Rev.* **2009**, *38*, 372−390.
(3) Lou, X. W.; Archer, L. A.; Yang, Z. C. *Adv. Mater.* **2008**, *20*, 3987−4019.
(4) Lai, X. Y.; Halpert, J. E.; Wang, D. *Energy Environ. Sci.* **2012**, *5*, 5604−5618.
(5) Hu, J.; Chen, M.; Fang, X. S.; Wu, L. M. *Chem. Soc. Rev.* **2011**, *40*, 5472−5491.
(6) Zhou, L.; Zhao, D.; Lou, X. W. *Adv. Mater.* **2012**, *24*, 745−748.
(7) Pan, A. Q.; Wu, H. B.; Yu, L.; Lou, X. W. *Angew. Chem., Int. Ed.* **2013**, *125*, 2282−2286.
(8) Li, H. X.; Bian, Z. F.; Zhu, J.; Zhang, D. Q.; Li, G. S.; Huo, Y. N.; Li, H.; Lu, Y. F. *J. Am. Chem. Soc.* **2007**, *129*, 8406−8407.
(9) Liu, J.; Qiao, S. Z.; Chen, J. S.; Lou, X. W.; Lu, X.; Xing, G. Q. *Chem. Commun.* **2011**, *47*, 12578−12591.
(10) Chen, D.; Zhang, H.; Hu, S.; Li, J. *J. Phys. Chem. C* **2008**, *112*, 117−122.
(11) Yuan, M.; Shan, Z.; Tian, B.; Tu, B.; Yang, P.; Zhao, D. *Microporous Mesoporous Mater.* **2005**, *78*, 37−41.
(12) Noy, A.; Miller, A. E.; Klare, J. E.; Weeks, B. L.; Woods, B. W.; DeYoreo, J. J. *Nano Lett.* **2002**, *2*, 109−112.
(13) Warule, S. S.; Chaudhari, N. S.; Kale, B. B.; Patil, K. R.; Koinkar, P. M.; More, M. A.; Murakamie, R. *J. Mater. Chem.* **2012**, *22*, 8887−8895.
(14) Agrawal, M.; Gupta, S.; Pich, A.; Zafeiropoulos, N. E.; Stamm, M. *Chem. Mater.* **2009**, *21*, 5343−5348.
(15) Huang, X.; Shang, L.; Chen, S.; Xia, J.; Qi, X. P.; Wang, X. C.; Zhang, T. R.; Meng, X. M. *Nanoscale* **2013**, *5*, 3828−3833.
(16) Qiao, L.; Wang, X. H.; Qiao, L.; Sun, X. L.; Li, X. W.; Zheng, Y. X.; He, D. Y. *Nanoscale* **2013**, *5*, 3037−3042.
(17) Freund, H. J.; Meijer, G.; Scheffler, M.; Schlcgl, R.; Wolf, M. *Angew. Chem., Int. Ed.* **2011**, *50*, 10064−10094.
(18) Somorjai, G. A.; Mccrea, K. R. *Adv. Catal.* **2000**, *45*, 385−438.
(19) Shou, M.; Tanaka, K.; Yoshioka, K.; Morooka, Y.; Nagano, S. *Catal. Today* **2004**, *90*, 255−261.
(20) Liu, X. W.; Zhou, K. B.; Wang, L.; Wang, B. Y.; Li, Y. D. *J. Am. Chem. Soc.* **2009**, *131*, 3140−3141.
(21) Esch, F.; Fabris, S.; Zhou, L.; Montini, T.; Africh, C.; Fornasiero, P.; Comelli, G.; Rosei, R. *Science* **2005**, *309*, 752−755.
(22) Guo, X. H.; Mao, C. C.; Zhang, J.; Huang, J.; Wang, W. N.; Deng, Y. H.; Wang, Y. Y.; Cao, Y.; Huang, W. X.; Yu, S. H. *Small* **2012**, *8*, 1515−1520.
(23) Qi, J.; Chen, J.; Li, G. D.; Li, S. X.; Gao, Y.; Tang, Z. Y. *Energy Environ. Sci.* **2012**, *5*, 8937−8941.
(24) Feng, Y. J.; Liu, L. L.; Wang, X. D. *J. Mater. Chem.* **2011**, *21*, 15442−15448.
(25) Wang, X.; Jiang, Z. Y.; Zheng, B. J.; Xie, Z. X.; Zheng, L. S. *CrystEngComm* **2012**, *14*, 7579−7582.
(26) Chen, G. Z.; Zhu, F. F.; Sun, X.; Sun, S. X.; Chen, R. P. *CrystEngComm* **2011**, *13*, 2904−2908.
(27) Yang, Z. J.; Han, D. Q.; Ma, D. L.; Liang, H.; Liu, L.; Yang, Y. Z. *Cryst. Growth Des.* **2010**, *10*, 291−295.
(28) Shen, G. L.; Liu, H. D.; Wang, Q.; Wang, Z.; Chen, Y. F. *J. Nanopart. Res.* **2012**, *14*, 954−961.
(29) Vayssieres, L.; Keis, K.; Hagfeldt, A.; Lindquist, S. E. *Chem. Mater.* **2001**, *13*, 4395−4398.
(30) Castillejos, E.; Bacsa, R.; Ruiz, A. G.; Datas, L.; Serp, P. *Nanoscale* **2011**, *3*, 929−932.
(31) Naknam, P.; Luengnaruemitchai, A.; Wongkasemjit, S. *Int. J. Hydrogen Energy* **2009**, *34*, 9838−9846.
(32) Carabineiro, S. A. C.; Machado, B. F.; Bacsa, R. R.; Serp, P.; Drazic, G.; Faria, J. L.; Figueiredo, J. L. *J. Catal.* **2010**, *273*, 191−198.
(33) Zhong, S. L.; Zhang, L. F.; Wang, L.; Huang, W. X.; Fan, C. M.; Xu, A. W. *J. Phys. Chem. C* **2012**, *116*, 13127−13132.
(34) Xie, Q. S.; Li, J. G.; Tian, Q.; Shi, R. R. *J. Mater. Chem.* **2012**, *22*, 13541−13547.
(35) Che, P.; Fang, D.; Zhang, D.; Feng, J.; Wang, J.; Hu, N.; Meng, J. *J. Coord. Chem.* **2005**, *58*, 1581−1588.
(36) Milanova, M. M.; Arnaudov, M. G.; Getsova, M. M.; Todorovsky, D. S. *J. Alloys Compd.* **1998**, *264*, 95−103.
(37) Demadis, K. D.; Coucouvanis, D. *Inorg. Chem.* **1995**, *34*, 436−488.
(38) Zhu, F. F.; Chen, G. Z.; Sun, S. X.; Sun, X. *J. Mater. Chem. A* **2013**, *1*, 288−294.
(39) Liu, X. F.; Yang, H. X.; Han, L.; Liu, W.; Zhang, C.; Zhang, X. Y.; Wang, S. P.; Yang, Y. Z. *CrystEngComm* **2013**, *15*, 7769−7775.
(40) Jiao, Y.; Wang, F. F.; Ma, X. M.; Tang, Q. H.; Wang, K.; Guo, Y. M.; Yang, L. *Microporous Mesoporous Mater.* **2013**, *176*, 1−7.
(41) Zhou, M. J.; Hu, Y.; Liu, Y.; Yang, W. L.; Qian, H. S. *CrystEngComm.* **2012**, *14*, 7686−7693.
(42) Meng, M.; Liu, Y. Q.; Sun, Z. S.; Zhang, L. J.; Wang, X. T. *Int. J. Hydrogen Energy* **2012**, *37*, 14133−14142.
(43) Zhang, R. R.; Ren, L. H.; Lu, A. H.; Li, W. C. *Catal. Commun.* **2011**, *13*, 18−21.
(44) Yu, Y.; Cao, C. Y.; Chen, Z.; Liu, H.; Li, P.; Dou, Z. F.; Song, W. G. *Chem. Commun.* **2013**, *49*, 3116−3118.
(45) Han, M. M.; Wang, X. J.; Shen, Y. N.; Tang, C. H.; Li, G. S.; Smith, R. L. *J. Phys. Chem. C* **2010**, *114*, 793−798.
(46) Shevchenko, E. V.; Bodnarchuk, M. I.; Kovalenko, M. V.; Talapin, D. V.; Smith, R. K.; Aloni, S.; Heiss, W.; Alivisatos, A. P. *Adv. Mater.* **2008**, *20*, 4323−4329.
(47) Eustis, S.; El-Sayed, M. A. *Chem. Soc. Rev.* **2006**, *35*, 209−217.
(48) Zhu, H. G.; Ma, Z.; Clark, J. C.; Pan, Z. W.; Overbury, S. H.; Dai, S. *Appl. Catal., A* **2007**, *326*, 89−99.
(49) Moreau, F.; Bond, G. C. *Catal. Today* **2006**, *114*, 362−368.